BioNanoScience (2023) 13:1885–1895
https://doi.org/10.1007/s12668-023-01149-3

Impact of Variable Metal Oxide Loadings on Photocatalytic and Antibacterial Behaviour of CNT-NiO Nanocomposites

Amanvir Singh[1] · Vikas Kaushik[2] · Vinay Kumari[3] · Arkaja Goswami[4] · Sonia Nain[1]

Accepted: 19 June 2023 / Published online: 19 July 2023

Abstract
In the present study, pure NiO NPs (Nickel oxide nanoparticles) along with their SWCNT (Single-walled carbon nanotubes) supported binary nanocomposites containing optimized wt% (weight percentages) of NiO 10%, NiO 20%, NiO 30%, and NiO 40% were synthesized via chemically controlled one-pot approach. The presence of characteristic Ni-O peak at 467 cm^{-1} in FTIR and fairly intense peaks in XRD data implied that synthesized NiO NPs exhibit crystallinity and don't involve impurity basis from pure Ni metal NPs. Further, the influence of variable NiO loadings on optical, morphological, photocatalytic, and antibacterial properties of the composites was explored using SEM, TEM, EDAX and UV-Visible spectroscopy. The composites were used as an effective photocatalyst for degrading MB (methylene blue) dye under UV illumination. The overall degradation behaviour of SWCNT/NiO nanocomposites initially increased with increase in NiO loading upto 30% and then showed a rapid downfall for catalyst with 40% NiO loading. The NiO 30% catalyst degraded 92.4% of the dye, whereas NiO 40% reduced the dye upto 84.2% of its initial concentration within 100 min of irradiation time. They showed better biocidal efficiency with determined activity against *S. aureus* and *E. coli*. The toxicity of NiO 40% was more pronounced against *E. coli* and *S. aureus*, as it exhibited 16.4 mm and 16 mm diameter of ZOI respectively against these strains. Overall, SWCNT/NiO 30% composites possess comparatively superior properties than pure NiO NPs and other NiO-loaded composites for their application in advancement of photocatalysis and anti-bacterial agents, thereby flooring an idea towards synthesis of multifunctional nanocomposites in the near future.

Keywords Antibacterial agents · Binary nanocomposites · Carbon nanotubes · NiO Nanoparticles · Photocatalysis

1 Introduction

Since the beginning of the twenty-first century, concerns associated with the discharge of household wastewater and toxic chemicals directly into rivers, ponds, lakes, etc. have gained universal attention. The presence of these toxic chemicals and pathogenic bacteria inside aquatic systems ultimately causes various life-threatening diseases in all forms of creatures. Even though all production-oriented industries are fairly responsible for this problem, but the heavy discharge of non-biodegradable organic dyes especially from photographic and textile-based industries is the major contaminant [1]. The chemicals left in industrial discharge react with other disinfectants, notably chlorine, to form carcinogenic by-products [2]. In addition, the colloidal matter attached with colorful dyes increases the foul smell and turbidity, which prevents deep penetration of sunlight along with reduced levels of oxygenation inside water bodies, finally upsetting the biological cycle of aquatic life. Being a part of the scientific community, it is our paramount responsibility to find workable solutions without hampering ongoing industrial growth. To date, researchers have employed several physical methods, including reverse

✉ Sonia Nain
sonianain.chem@dcrustm.org

[1] Department of Chemistry, Deenbandhu Chhotu Ram University of Science and Technology, Murthal, Haryana 131039, India

[2] Department of Biotechnology, Deenbandhu Chhotu Ram University of Science and Technology, Murthal, Sonipat, India

[3] Department of Applied Sciences, Panipat Institute of Engineering and Technology, Panipat, Haryana 132102, India

[4] Department of Chemistry, Shyamlal College, University of Delhi, New Delhi 110032, India

osmosis, coagulation, aerobic and anaerobic biological treatment, and use of adsorbents to remove harmful dyes, such as methylene blue (MB), rose bengal (RB), phenol red (PR), para nitrophenol (PNP), methyl orange (MO), and azo dyes [3]. All these methods are either expensive or tunable only to low levels of contaminant concentration in comparison to metal oxide semiconductor–based photocatalysis.

Carbon material/metal oxide–based nanocomposites have been established as promising materials for energy storage, bio-sensing, photocatalysis, hydrogen storage, and various medical applications owing to their outstanding physical as well as chemical properties [4–7]. The success of multifunctional composites depends undoubtedly on the inherent properties of the material being employed within the composites. It is also a widely recognized concept that "structure dictates function"; hence, a good photocatalyst as well as antibacterial agent must possess properties like large surface area, smaller size, desirable band gap, high stability and easy perturbation tendency without agglomerate formation when attached to a support [8–10]. In recent years, NiO composites synthesized via different synthesis routes were explored separately for their use in photocatalytic and antibacterial applications. Thereby, H. Duan et al. synthesized NiO nanoparticles (NPs) via solution phase reaction in oxygen atmosphere. These NPs degraded rhodamine B dye in 180 min [11]. While, K.S. Khashan et al. reported the synthesis of colloidal NiO NPs via pulsed laser ablation method. The spherical-shaped NPs showed zone of inhibition (ZOI) values equal to 12.6±0.57 and 14.3±1.15 mm against *S. aureus* and *E. coli* respectively [12]. A. Ezhilarasi and co-workers reported crystalline NiO NPs synthesized via green synthesis route. The NPs were more pronounced for gram positive bacterial strains and completely mineralized 4-CP dye within 210 min [13]. Furthermore, X.N. Liao et al. prepared carbon nanotube (CNT) coated NiO NPs via chemical precipitation method. The resulting composite depicted better catalytic activity than reduced NiO/graphite for benzene hydrogenation reactions [14]. But all these methods didn't focus on the synthesis of composites with tailored ingredients that could become one stop solution for wastewater treatment alongside abatement of pathogenic bacteria (Table 1).

Here, we account for the synthesis of pure as well as SWCNT supported NiO NPs with variable weight percentages of NiO NPs, i.e. NiO 10%, NiO 20%, NiO 30% and NiO 40% using one-pot synthesis approach. The composites were first investigated for their potential application in the arena of wastewater treatment, and then the remaining composite residues after dye degradation were used to explore their antibacterial performance. An understanding into the role of NiO NPs and CNTs in enhancing the catalytic and biocidal potential of SWCNT/NiO nanocomposite was developed to justify the multifunctional capabilities of synthesized composites.

2 Materials and Methods

2.1 Chemicals and Reagents

NiO NPs and their respective nanocomposites with varying weight percentages were synthesized using the following analytical grade chemicals purchased from Merck (Germany): nickel chloride hexahydrate ($NiCl_2.6H_2O$), potassium hydroxide (KOH), absolute ethanol (C_2H_5OH), hydrazine hydrate (NH_2NH_2), sulphuric acid (H_2SO_4), and nitric acid (HNO_3). SWCNTs with avg. length: 4–8 µm were bought from Nanoshel, USA.

2.2 Fabrication of SWCNT/NiO Nanocomposite

Firstly, SWCNTs were activated in 3:1 (H_2SO_4:HNO_3) acid solution and then they were used as a template for heterogeneous nucleation of NiO nanoparticles above their mesoporous surface. The SWCNT/NiO nanocomposites were synthesized using modified one-pot synthesis approach [15]. Calculated amount of $NiCl_2.6H_2O$ was dissolved in ethanol and sonicated for 15 min. Secondly, NH_2NH_2 was dissolved in KOH in a separate beaker. Both, these solutions were mixed immediately with continuous magnetic stirring. The color of this solution started changing from green to milky blue due to formation of coordinate complexes of Ni inside the medium (Fig. 1). Prior to complete formation of NiO NPs, activated SWCNTs (sonicated for 10 min) were added to above solution without disturbing the ongoing reactions. After some time, color of the solution turned dark black. Thus, indicating the formation and attachment of NiO NPs over SWCNT surface. The obtained precipitates were washed several times using doubly distilled water and ethyl alcohol. Then they were calcinated for 3 h under 400 °C to achieve SWCNT/NiO-based binary nanocomposite. The desired composites containing 10%, 20%, 30% and 40% of NiO loading were acquired using the similar procedure as mentioned above.

2.3 Characterizations

The binary nanocomposites of SWCNT/NiO were characterized via FTIR using Perkin Elmer-Fourier Transform Infra-Red spectrometer for functional group analysis. XRD was recorded on Rigaku X-Ray Diffractometer containing CuKα X-ray source with wavelength λ = 1.54 Å for phase analysis. Morphological studies were explored with Field Emission Scanning Electron Microscopy (FESEM) using HITACHI

Table 1 Comparison of some excellent multifunctional photocatalysts previously reported for degradation of toxic dyes

Catalyst	Light source	Dye	Irradiation time (in min)	Degradation efficiency (in %)	Reference
ZnS	*UV-vis.*	*MB*	*120*	*94.68 %*	[29]
CdO-CuO-ZnO	*UV-vis.*	*Alizarin red*	*120*	*93 %*	[30]
RuO_2/SWCNT	*UV-vis.*	*MB*	*100*	*92.6%*	[31]
NiO-CYO-CSO	*UV-vis.*	*CR*	*150*	*93%*	[32]
GO/Ag	*UV-vis.*	*MB*	*120*	*87.6%*	[33]
CYO-CSO	*UV-vis.*	*MB*	*120*	*93%*	[34]

(SU-8010) and Transmission Electron Microscopy (TEM) using Thermoscientific-Talos TEM. EDAX data was also obtained to analyze the elemental composition of the binary composites. Furthermore, LABINDIA UV-3092 Spectrophotometer was used for investigating catalytic absorption measurements of MB dye at different time intervals.

2.4 Photo-catalytic Activities Assays

The photocatalytic degradation experiments were performed under UV light (300 W/bulb, $\lambda = 365$ nm) for mineralizing MB dye. Initially, 0.07 g of SWCNT/NiO catalyst was dissolved in a beaker containing 70 mL solution of the dye. Then, the solution was kept in complete darkness with constant magnetic stirring to achieve adsorption-desorption equilibrium [16]. After 60 min the beaker was placed in UV-irradiated chamber and small amount of aliquot were gathered from it at an interval of 20 min each. The absorption spectrum of the supernatant liquid was analyzed between 500 and 800 nm to conclude the percentage degradation for dye solution.

2.5 Antibacterial Activity Assay

Antibacterial potential of different SWCNT/NiO nanocomposites was screened by agar well diffusion method [17], where commercially available antibiotic (Tetracycline) and ethanol were applied as positive and negative control respectively. The size of diameter of the transparent region called "zone of inhibition" and minimum inhibitory concentration (MIC) calculated using broth dilution method [18] were analyzed to achieve the biocidal efficiency of synthesized composite against selected bacterial strains.

3 Results and Discussion

3.1 FTIR Spectra

Figure 2 shows the FTIR spectra of pure NiO NPs and their binary composites with functionalized SWCNTs. Occurrence of V-shaped wide absorption band between 3680 and 3250 cm^{-1} could be attributed to O-H groups

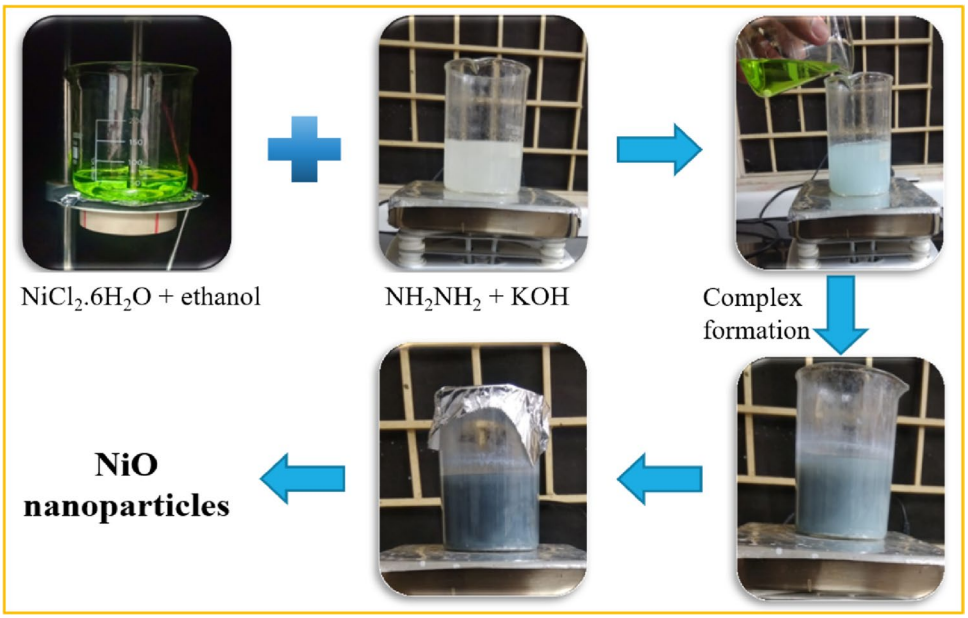

Fig. 1 Schematic representation of synthesis of NiO nanoparticles in absence of CNTs

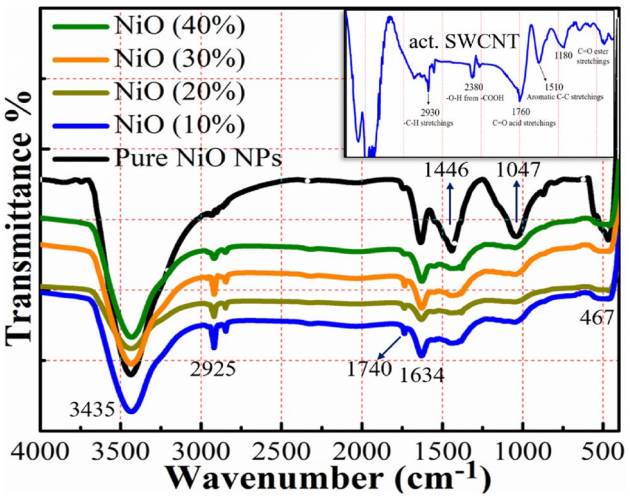

Fig. 2 FTIR spectra of pure NiO NPs and SWCNT/NiO based binary nanocomposites at different weight percentages

of functionalized SWCNTs or moisture absorbed on the sample due to FTIR measurements through KBr pellet technique (KBr is hygroscopic). The presence of striking peaks at 2925, 2854, 1740 and 1446 cm^{-1} in all compositions corresponds to C-H symmetric stretchings, C-H asymmetric stretchings, C=O stretchings and C-H bending vibrations respectively [19]. The characteristic peak for Ni-O bond was observed around 467 cm^{-1} for all the samples. However, upon nucleation of NiO NPs over SWCNT surface, all the characteristic peak intensities of M-O bond were reduced significantly, indicating the existence of interactions between NiO NPs and act. SWCNTs.

3.2 XRD Analysis

XRD characterization was performed to evaluate the crystal structure of SWCNT/NiO catalysts. Figure 3 shows characteristic peaks at 37.4°, 43.7°, 61.3°, 75.9°, and 79.2° for (111), (200), (220), (311), and (222) crystallographic planes of NiO NPs whereas minor peak at $2\theta = 26.2°$ is associated with the presence of (002) plane from graphitic carbon chains within the composites [20]. This observed data can be indexed to JCPDS card no. 47-1049 and dominance of pure NiO NPs without any impurity traces from $Ni(OH)_2$. Moreover, in respect of height of peaks for different NiO loadings, the characteristic peak intensities for NiO kept on rising with increase in NiO content from 10 to 40% while the CNT peak at 26.2° (inset of Fig. 3) was reducing gradually. This reduced appearance could be ascribed to the coating of NiO NPs over CNT surface that significantly covers the composite from diffraction. According to Debye-Scherrer equation: $D = k\lambda/\beta\cos\theta$ [21] applied on most intense (200) plane, the average size of bare NiO NPs was found 11 nm which was 1–2 nm larger than the NiO present inside the composites (Table 2). Hence, this abundance of smaller average NiO size could be favorable for higher specific surface area, more bacteria-composite aggregate formation and significantly enhanced dye adsorption.

3.3 Surface Morphology and Composition Analysis

In order to analyze the surface morphology, SEM was preferred. As shown in Fig. 4(a, b), the shape of synthesized NiO NPs was found spherical and F. Fazlali et al. [22] had also previously reported that spherical NiO NPs showed better photocatalytic activity than flower, plate and wooden NPs synthesized via thermal decomposition, sol-gel and hydrothermal routes respectively. The average particle size (inset of Fig. 4b) evaluated from the micrographs lies near 11 nm for bare NiO NPs and between 9 and 11 nm inside composites containing variable weight percentages of SWCNT/NiO composites (Table 2). Thus, examined particle sizes are in good corroboration with the results obtained from XRD data. The size variations in NP size could arise as a result of interparticular attrition during extended ultrasonication and availability of SWCNT surface for heterogeneous nucleation of NiO NPs. The addition of CNTs also prevented the self-agglomeration of NPs and proved advantageous while studying multifunctional properties of these composites. Moreover, the investigation of EDAX spectra (Fig. 5) clearly validated that the synthesized composites contained no impurity elements and are primarily composed of Ni, O and C.

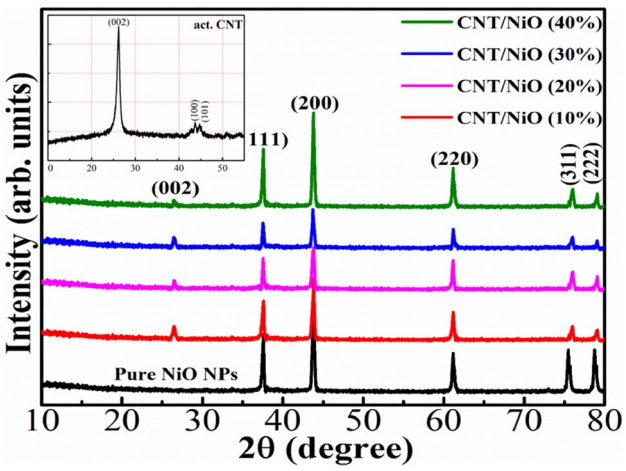

Fig. 3 XRD pattern of functionalized SWCNT (inset), pure NiO NPs and their binary nanocomposites at variable weight percentages

Table 2 Parameters calculated from photodegradation of MB dye with pure NiO nanoparticles and SWCNT/NiO based different photocatalysts

Samples	Crystallite size (nm)	% Degradation (in 100 min)	k (min^{-1})	R^2	$t_{1/2}$ (min)
Pure NiO NPs	11.04	70.6	0.01231	0.9511	56.29
SWCNT/NiO (10%)	10.86	82.4	0.01684	0.9727	41.15
SWCNT/NiO (20%)	10.03	86	0.01931	0.9815	35.88
SWCNT/NiO (30%)	9.61	92.4	0.02459	0.9944	28.18
SWCNT/NiO (40%)	9.42	84.2	0.01833	0.9912	37.80

3.4 TEM Analysis

TEM was performed to further validate the attaching of spherical NiO nanoparticles over SWCNTs. Fig. 6(a, b) exhibited the TEM micrographs of pure NiO NPs, which were further distributed uniformly over SWCNTs at different values of weight percentages (10–40%). On the contrary, as we kept on increasing the weight percentages, the NPs started re-agglomeration even in the presence of SWCNT template due to magnetic interactions between NiO NPs, as shown in Fig. 6(f). These interactions suppressed the nucleation effect of CNT template after 30% NiO loading and could hamper the multifunctional potential of synthesized composites due to non-availability of nanoparticle surface trapped inside the agglomerate core for reactive oxygen species generation.

3.5 Photocatalytic Degradation

Successive experiments were performed in UV-irradiated chambers to explore the photocatalytic behaviour of

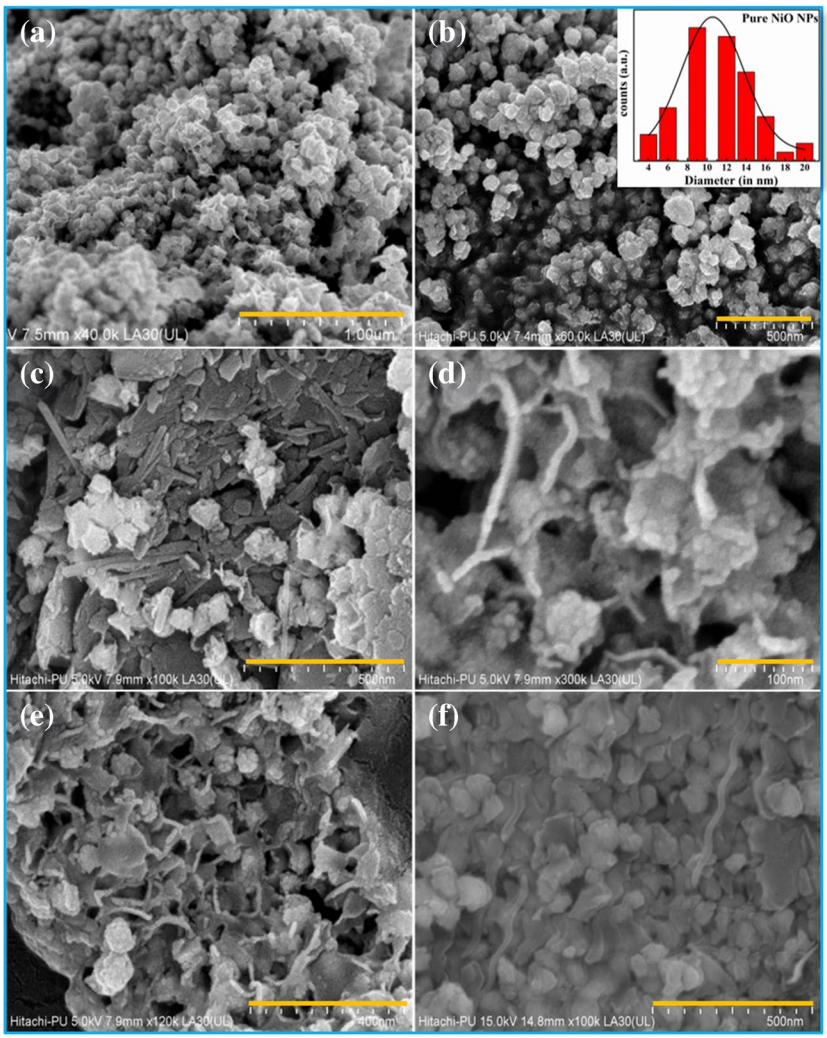

Fig. 4 SEM images of (**a**, **b**) pure NiO NPs and (**c**–**f**) different SWCNT/NiO composites, inset of (**b**) particle size histogram of pure NiO NPs

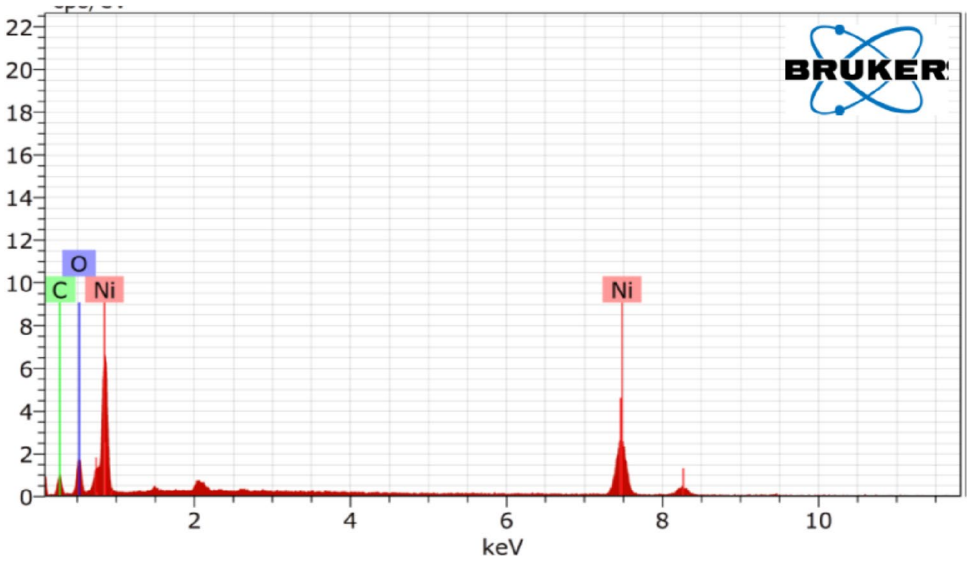

Fig. 5 EDX spectrum of SWCNT/NiO based binary nanocomposite

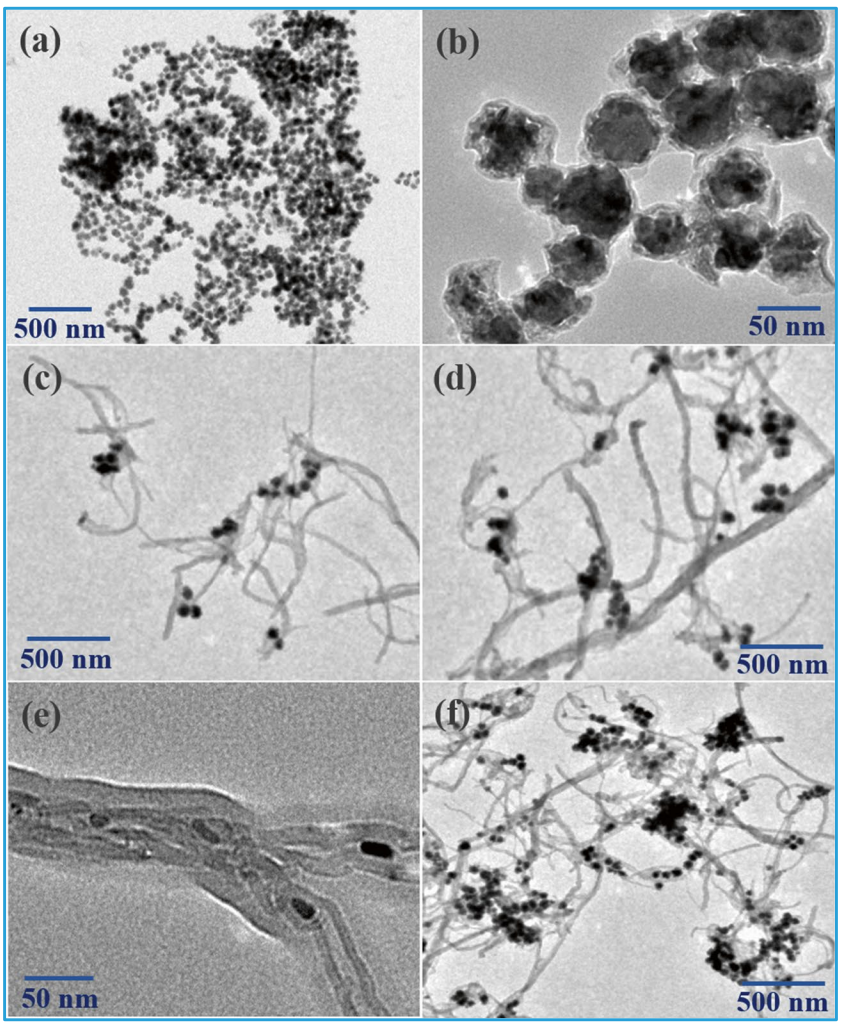

Fig. 6 TEM micrographs of (**a**, **b**) pure NiO NPs and (**c**–**f**) SWCNT supported NiO nanocomposites at different wt% of NiO NPs

NiO-supported SWCNT nanocomposites for degradation of MB dye. As shown in Fig. 7, the absorption spectra of MB dye exhibited gradual decrease in characteristic peak intensity, which verifies that the dye is being mineralized by the photocatalyst with the passage of time. The percentage degradation for bare NiO was found 70.6%. However, introduction of SWCNT prevented the self-agglomeration and provided a template for even adsorption of dye molecules, thus improving the inclusive degradation potential of synthesized photocatalysts. As demonstrated, the degradation behaviour of SWCNT/NiO nanocomposite initially improved with increase in NiO loading upto 30% and then showed rapid downfall for NiO 40% catalyst. The NiO 30% catalyst degraded 92.4% dye, whereas NiO 40% mineralized the dye upto 84.2% of its initial concentration within 100 min of UV exposure time.

It is clearly evident from Fig. 8(a) and adsorption curves that binary nanocomposites possess better degradation efficiencies in comparison to bare NiO NPs and activated SWCNTs, indicating the presence of SWCNT as support material to enhance the photocatalytic potential of synthesized catalysts [23–26]. According to literature, the optical band gap values for functionalized SWCNTs lies between 1.9 and 2.5 eV [27, 28]. However, the synergistic effect exerted by low band gap value of SWCNT counterbalanced the high band gap, i.e. 3.82 eV of pure NiO NPs thereby resulting into optimum values of 2.68 eV in binary composites carrying 30% NiO loading (Fig. 8b). Such optimum band gap values favored easy excitation of electrons from valence band (VB) to conduction band (CB), thereby generating abundant electron-hole pairs for redox processes. The photoexcited electrons in CB are trapped within

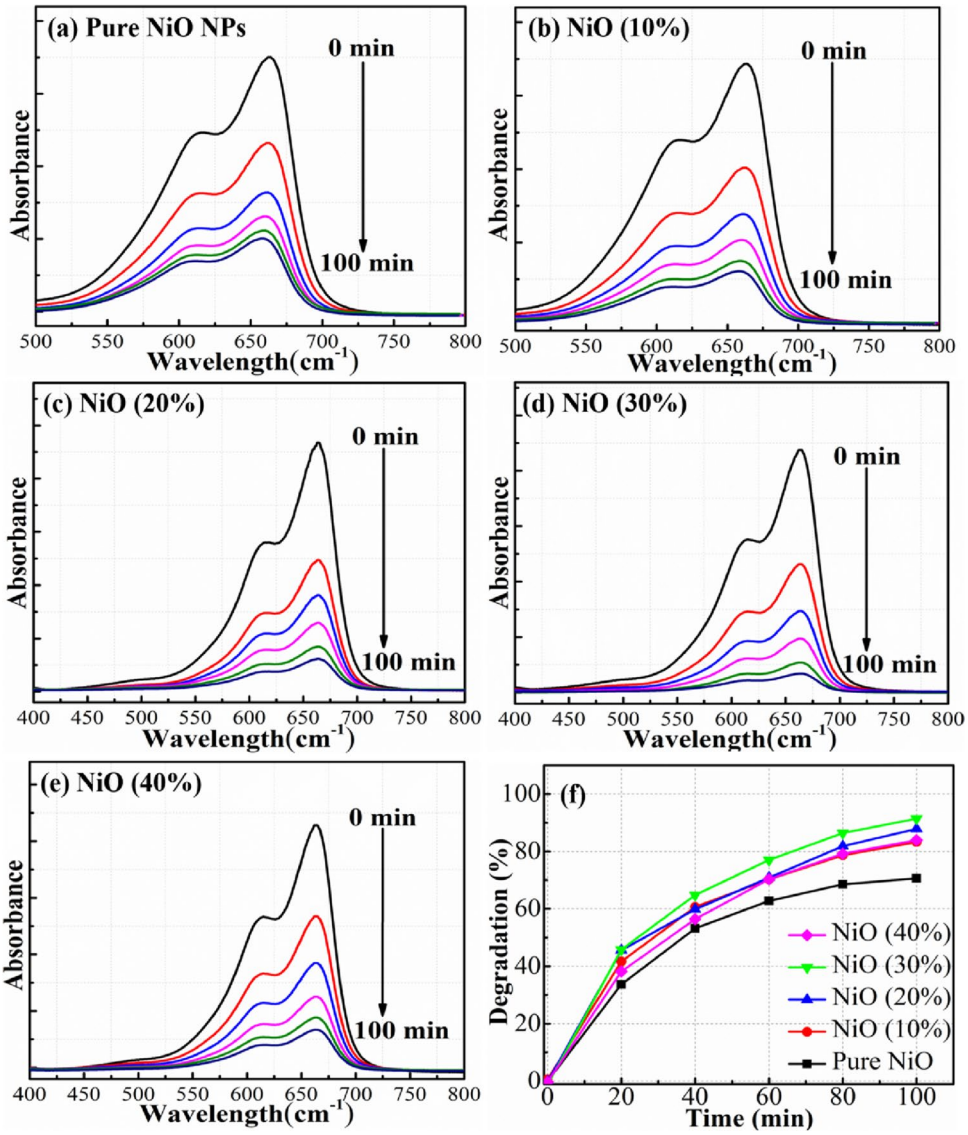

Fig. 7 (**a**–**e**) Absorption spectra and (**f**) % degradation of MB dye with NiO nanoparticles and different SWCNT/NiO nanocomposites as catalyst

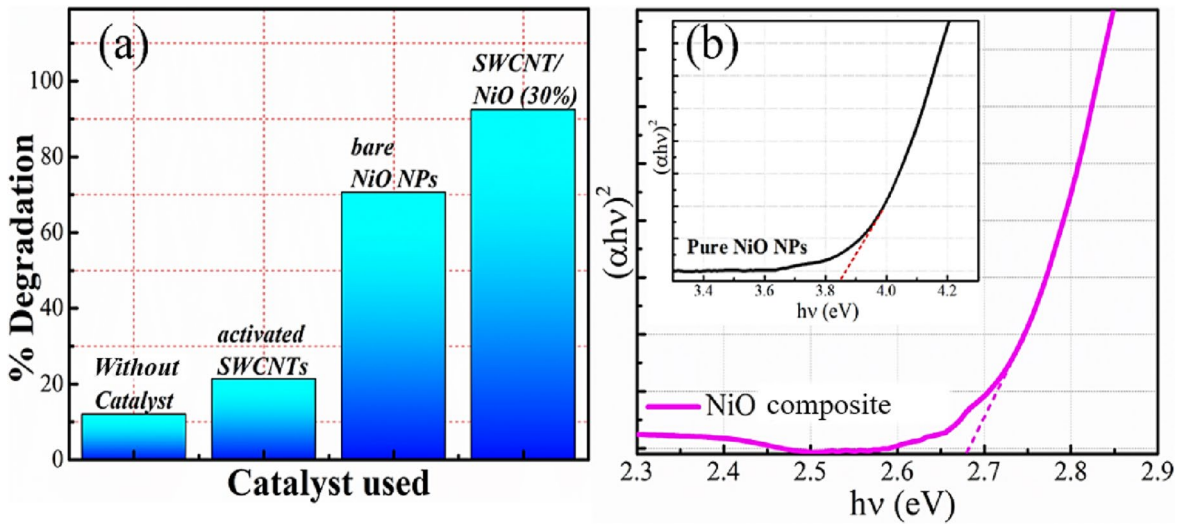

Fig. 8 (**a**) Comparison between different catalysts for degradation of MB dye inside 100 min. (**b**) Tauc plot of pure NiO and SWCNT/NiO (30%) composite

highly interconnected carbon channels of the support, thus hampering their de-excitation process. As a result of moderately increased electron-hole recombination time, the excited electrons get suitable time to react with available O_2 molecules to generate superoxide radicals likewise, the holes available in VB combines with H_2O molecules to generate hydroxyl radicals. All these reactive radicals initiate in situ generation of ROS that simultaneously attack and break down MB dye molecules adsorbed on the surface of SWCNT/NiO catalyst into less harmful by-products. The proposed mechanism can be understood in terms of undermentioned simple equations:

$$NiO + h\nu \rightarrow NiO\left(e_{CB}^{-} + h_{VB}^{+}\right) \quad (1)$$

$$NiO\left(e_{CB}^{-}\right) + SWCNT \rightarrow NiO^{+} + SWCNT(e^{-}) \quad (2)$$

$$NiO^{+} - SWCNT(e^{-}) + O_2 \rightarrow NiO^{+}/SWCNT + O_2^{-} \quad (3)$$

$$NiO\left(h_{VB}^{+}\right) + H_2O \rightarrow HO^{\cdot}(hydroxyl\ radical) + NiO \quad (4)$$

$$O_2^{-} + H^{+} \rightarrow HOO^{\cdot}(perhydroxyl\ radical) \quad (5)$$

$$HO^{\cdot} + HO^{\cdot} \rightarrow H_2O_2\ (peroxide) \quad (6)$$

$$ROS\left(O_2^{-}, HO^{\cdot}, H_2O_2\right) + adsorbed\ dye \rightarrow H_2O + CO_2 + degraded\ dye \quad (7)$$

Another purposeful information worth to be noted is that even in the presence of similar reaction conditions, the degradation efficiencies of SWCNT/NiO-based photocatalysts were not increasing with increase in NiO loading. The degradation tendency started slowing down after using catalyst above 30% metal oxide loading, not because of excessive loading of NiO NPs but as a result of domination by weak magnetic interactions between NiO NPs. After 30% NiO loading, the magnetic NPs started attracting each other, thus barricading the incident UV light from interacting with NPs trapped inside agglomerated core, leading to inferior efficiencies of SWCNT/NiO (40%) photocatalysts. Furthermore, the rate constant k and correlation coefficient R^2 for degradation of MB dye by all the synthesized catalysts were also evaluated after linear fittings of the plot between $-\ln c/c_0$ and irradiation time (Fig. 9) and it established that all the dye degradation processes performed here followed pseudo first-order kinetics, as R^2 values lie between 0.95 and 1. The half-life time ($t_{1/2}$) values calculated for first order reactions, i.e. $t_{1/2} = 0.693/k$ finally established that SWCNT/NiO (30%) nanocomposite generated ROS more quickly which finally degraded the 10 ppm solution of MB dye upto 50% of its initial concentration within 28 min. Thus, SWCNT/NiO (30%) composite could be regarded as a better option than all other synthesized binary nanocomposites of SWCNT/NiO for degrading the dyes.

3.6 Antibacterial Investigation

The antibacterial potential of as synthesized SWCNT/NiO nanocomposites and bare NiO NPs was assessed against two Gram-negative and two Gram-positive strains. For this purpose, the concentration of composite was taken at 25 µg/mL and the ZOI values measured from the hinderance of bacterial strain was depicted in Fig. 10. It was observed

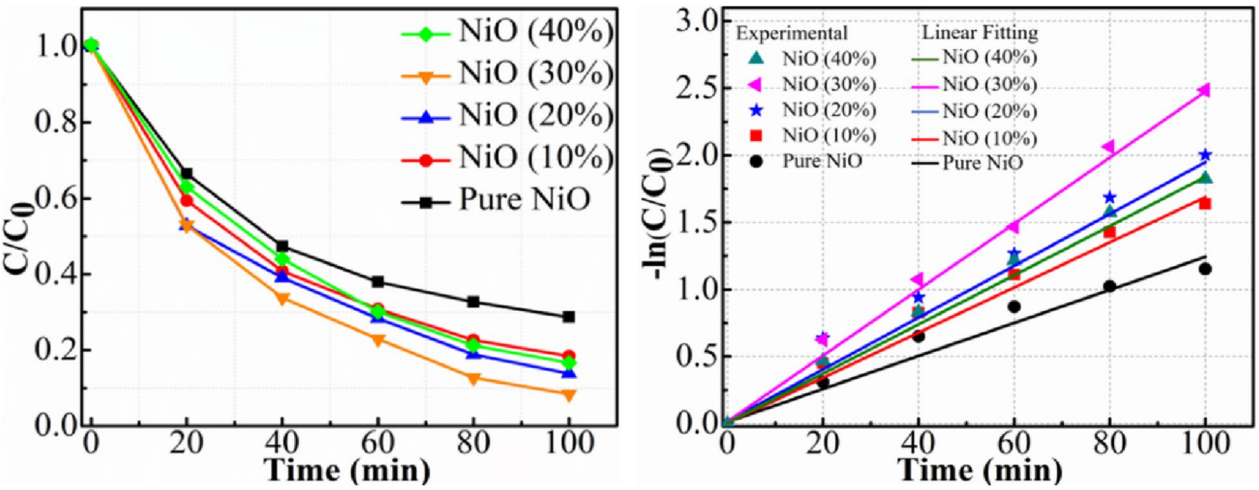

Fig. 9 C/C_0 v/s time and linearly fitted plots of $-\ln(C/C_0)$ v/s time for degradation of MB dye with pure NiO nanoparticles and different SWCNT/NiO nanocomposite catalysts

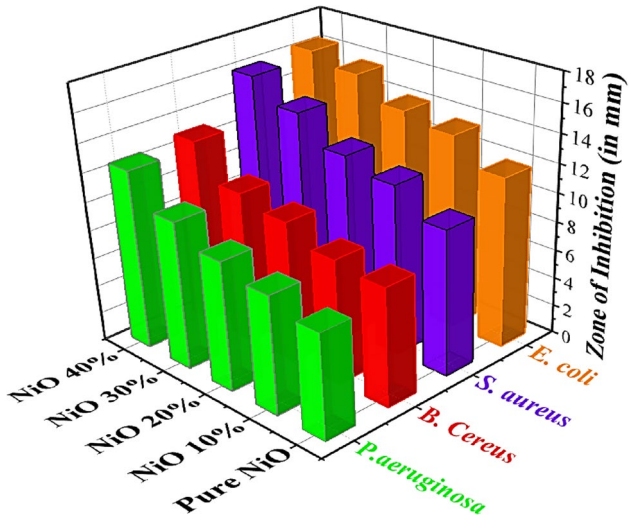

Fig. 10 Zone of inhibition values of pure NiO nanoparticles and SWCNT/NiO based binary composites against selected bacterial strains

that synthesized binary nanocomposite containing 40% NiO loading was more effective against *Staphylococcus aureus* (16 mm) and *Escherichia coli* (16.4 mm), however it also repressed the growth of *Bacillus cereus* (13 mm) and *Pseudomonas aeruginosa* (12.6 mm). These significantly improved biocidal effects could be accredited to the smaller size and synergistic effect of NiO-loaded SWCNTs, as smaller size enhances the dispersibility and permeability of extracellular NiO inside bacterial cell [35], the CNTs could rupture cell wall through its sharp tips and produce oxidative stress on trapped bacterial body [36], thereby accompanying the entrance of NiO NPs inside bacterial cell. After crossing the cell membrane NiO NPs interacts with mesosomes and

Table 3 MIC values of pure NiO and SWCNT/NiO nanocomposite against selected bacterial strains

S. no.	Bacterial strains	SWCNT/NiO (40%)	Pure NiO
1	*E. coli* (MTCC 9721)	0.04 mg/mL	0.78 mg/mL
2	*P. aeruginosa* (MTCC 3542)	0.19 mg/mL	1.56 mg/mL
3	*S. aureus* (MTCC 11949)	0.09 mg/mL	0.78 mg/mL
4	*B. cereus* (MTCC 1272)	0.39 mg/mL	3.12 mg/mL

other cellular organelles to generate $\dot{O}H$ and $\bullet O_2^-$, having strong antibacterial effects [37]. These reactive radical species along with Ni^{2+} ions check DNA replication and ATP production [38]. All these major biological deficits become tough challenges for survival and mutation, the bacterial strain is not able to create a defense mechanism to counter these collateral damages and lastly succumbs to the biocidal effects of synthesized SWCNT/NiO composites.

To further substantiate the ZOI results, 2X Broth dilution method was applied to find out the minimum concentration at which the synthesized composite successfully inhibited the growth of selected bacterial strains. From the experiments, it was concluded that synthesized SWCNT/NiO (40%) composite exhibited least MIC value of 0.04 and 0.09 mg/mL against both *E. coli* and *S. aureus* respectively. However, pure NiO NPs displayed least MIC values of 0.781 mg/mL against these strains. As depicted in Table 3, bare NiO NPs were found to be more efficient against *E. coli* and *S. aureus* with MIC value of 0.78 mg/mL in comparison to other strains. The presence of thick peptidoglycan layer on *B. cereus* resisted the antibacterial activity of NiO NPs and its binary composite to considerable extent, thus showing comparatively high inhibitory

concentrations [39]. Finally, obtained MIC values are in well agreement with the values evaluated after measuring the diameter of ZOI. For this reason, it can be concluded that both SWCNTs and NiO NPs are potential antibacterial agents; however, their binary composites containing high NiO loading act synergistically with porous SWCNT support to form Bacteria-CNT aggregates [40, 41]. These aggregates provide close proximity and improved chances of nanoparticular interaction with cellular organelles, thereby leading to enhanced antibacterial performance.

4 Conclusion

Pure as well as SWCNT decorated NiO NPs with variable NiO loading ranging from 10 to 40% were synthesized for analyzing their antibacterial and photocatalytic behaviour towards degradation of MB dye. The study of FTIR data showed characteristic peaks for Ni-O bond vibration at 467 cm^{-1}, XRD data with sharp and intense peaks confirmed long range crystallinity order and EDAX established that synthesized composites are composed of Ni, O and C elements. The microstructural analysis revealed that NiO NPs are spherical and lies in small size range. It also elucidated that acid functionalized SWCNTs acted as a template and provided nucleation sites for heterogeneous nucleation of spherical NiO NPs. Compared to pure NiO NPs and activated SWCNTs, the synthesized binary nanocomposite with 30% NiO loading behaved as good photocatalyst and degraded 92.6% of MB dye within 100 min. On the contrary, when tested for their antibacterial potential, composite with 40% NiO loading showed strong antibacterial activities at rather low dose (0.04 mg/mL against *E. coli*). The toxicity of SWCNT/NiO (40%) was more pronounced against *E. coli* and *S. aureus*, as it exhibited 16.4 mm and 16 mm diameter of ZOI respectively against these strains. This ambiguity in results could be attributed to the dominance of weak magnetic forces between NiO NPs after 30% loading. Finally, this idea of synthesizing multifunctional nanocomposites could ultimately enhance the fabrication of engineered nanocomposites that could be applicable in multiple fields in near future.

Author Contributions Amanvir Singh: Conceptualization, Formal analysis, Investigation, Writing- Original draft preparation. Vikas Kaushik: Software, Validation, Formal analysis, Antibacterial assay.

Vinay Kumari: Data curation and investigation. Arkaja Goswami and Sonia Nain: Conceptualization, Formal analysis, Investigation, Supervision, Reviewing and Editing.

Data Availability No separate data sets are used. All the information and data has been provided in this word file.

Declarations

Ethics Approval No approval was required as no experiments were carried out on human or animal tissues.

Competing Interests The authors declare no competing interests.

References

1. Dong, C., Lu, J., Qiu, B., Shen, B., Xing, M., & Zhang, J. (2018). Developing stretchable and graphene-oxide-based hydrogel for the removal of organic pollutants and metal ions. *Applied Catalysis B: Environmental, 222*(1), 146–156.
2. Richardson, S., & Postigo, C. (2011). In M. Lazaridis & I. Colbeck (Eds.), *The handbook of environmental chemistry* (Vol. 20, pp. 93–137). Springer.
3. Natrajan, S., Bajaj, H. C., & Tayade, R. J. (2018). Recent advances based on the synergetic effect of adsorption for removal of dyes from waste water using photocatalytic process. *Journal of Environmental Sciences, 65*(1), 201–222.
4. You, B., Wang, L., Yao, L., & Yang, J. (2013). Three dimensional N-doped graphene–CNT networks for supercapacitor. *Chemical Communications, 49*(44), 5016–5021.
5. Singh, A., Goswami, A., & Nain, S. (2020). Enhanced antibacterial activity and photo-remediation of toxic dyes using Ag/SWCNT/PPy based nanocomposite with core–shell structure. *Applied Nanoscience, 10*(7), 2255–2268.
6. Chinnaiah, K., Maik, V., Kannan, K., Potemkin, V., Grishina, M., Gohulkumar, M., Tiwari, R., & Gurushankar, K. (2022). Experimental and Theoretical Studies of Green Synthesized Cu 2 O Nanoparticles Using Datura Metel L. *Journal of Fluorescence, 32*, 559–568.
7. Huang, J., Li, Y., Xu, Z., Li, W., Xu, B., Meng, H., & Guo, W. (2019). An integrated smart heating control system based on sandwich-structural textiles. *Nanotechnology, 30*, 325203.
8. Wang, X., Blechert, S., & Antonietti, M. (2012). Polymeric graphitic carbon nitride for heterogeneous photocatalysis. *ACS Catalysis, 2*(8), 1596–1606.
9. Song, B., Wang, T., Sun, H., Shao, Q., Zhao, J., Song, K., Hao, L., Wang, L., & Guo, Z. (2017). Two-step hydrothermally synthesized carbon nanodots/WO 3 photocatalysts with enhanced photocatalytic performance. *Dalton Transactions, 46*(45), 15769–15777.
10. Jiang, Y., Sun, J., & Wu, S. (2017). BiOCl nanosheets with controlled exposed facets and improved photocatalytic activity. *Catalysis Letters, 147*, 2006–2012.
11. Duan, H., Zheng, X., Yuan, S., Li, Y., Tian, Z., Deng, Z., & Su, B. (2012). Sub-3 nm NiO nanoparticles: Controlled synthesis, and photocatalytic activity. *Materials Letters, 81*, 245–247.
12. Khashan, K. S., Sulaiman, G. M., Hamad, A. H., Abdulameer, F. A., & Hadi, A. (2017). Generation of NiO nanoparticles via pulsed laser ablation in deionised water and their antibacterial activity. *Applied Physics A, 123*, 1–10.
13. Ezhilarasi, A., Vijaya, J. J., Kaviyarasu, K., Kennedy, L., Jothiramalingam, R., Lohedan, H. A., & Photochem, J. (2018). Green synthesis of NiO nanoparticles using Aegle marmelos leaf extract for the evaluation of in-vitro cytotoxicity, antibacterial and photocatalytic properties. *Journal of Photochemistry and Photobiology B: Biology, 180*, 39–50.
14. Liao, X. N., Wang, Q. L., Hu, C. Y., & Li, F. Y. (2009). Preparation of NiO/MWNTs nanocomposites by a simple chemical

precipitation method. *Journal of the Chinese Chemical Society, 56*, 475–479.
15. Hayashi, Y. (2016). Pot economy and one-pot synthesis. *Chemical Science, 7*, 866–880.
16. Li, Q., Kako, T., & Ye, J. (2010). Strong adsorption and effective photocatalytic activities of one-dimensional nano-structured silver titanates. *Applied Catalysis A: General, 375*(1), 85–91.
17. Athanassiadis, B., Abbott, P. V., George, N., & Walsh, L. J. (2009). An in vitro study of the antimicrobial activity of some endodontic medicaments and their bases using an agar well diffusion assay. *Australian Dental Journal, 54*(2), 141–146.
18. Kaushik, V., Singh, A., Arya, A., Sindhu, S., Sindhu, A., & Singh, A. (2020). Enhanced production of cordycepin in Ophiocordyceps sinensis using growth supplements under submerged conditions. *Biotechnology Reports, 28*, e00557.
19. Sannasi, V., Maheswari, K., Karthikeyan, C., & Karuppuchamy, S. (2020). H_2O_2 -assisted microwave synthesis of NiO/CNT nanocomposite material for supercapacitor applications. *Ionics, 1*, 1–13.
20. Liu, J., Zhang, Y., Zhang, L., Xie, F., Vasileff, A., & Qiao, S. (2019). Graphitic carbon nitride (g-C3N4)-derived N-rich graphene with tuneable interlayer distance as a high-rate anode for sodium-ion batteries. *Advanced Materials, 31*(24), 1901261.
21. Holzwarth, U., & Gibson, N. (2011). The Scherrer equation versus the Debye-Scherrer equation. *Nature Nanotechnology, 6*(9), 534–535.
22. Fazlali, F., Mahjoub, A. R., & Abazari, R. (2015). A new route for synthesis of spherical NiO nanoparticles via emulsion nanoreactors with enhanced photocatalytic activity. *Solid State Sciences, 48*, 263–269.
23. Woan, K., Pyrgiotakis, G., & Sigmund, W. (2009). Photocatalytic carbon-nanotube–TiO2 composites. *Advanced Materials, 21*(21), 2233–2239.
24. Sapkota, K. P., Lee, I., Hanif, M., Islam, M., & Haua, J. (2019). Solar-Light-Driven Efficient ZnO–Single-Walled Carbon Nanotube Photocatalyst for the Degradation of aPersistent Water Pollutant Organic Dye. *Catalysts, 9*(6), 498–502.
25. Weng, B., Liu, S., Zhang, N., Tang, Z., & Xu, Y. (2014). A simple yet efficient visible-light-driven CdS nanowires-carbon nanotube 1D–1D nanocomposite photocatalyst. *Journal of Catalysis, 309*, 146–155.
26. Xu, Y., Xu, H., Yan, J., Li, H., Huang, L., Zhang, Q., Huang, C., & Wan, H. (2013). A novel visible-light-response plasmonic photocatalyst CNT/Ag/AgBr and its photocatalytic properties. *Physical Chemistry Chemical Physics, 15*, 5821–5830.
27. Gross, M. L., & Hickner, M. A. (2010). Using cyclic voltammetry to measure bandgap modulation of functionalized carbon nanotubes. *Electrochemical and Solid-State Letters, 13*(2), K5–K7.
28. Niranjan, M. K. (2020). Theoretical investigation of electronic bandgaps of semiconducting single-walled carbon nanotubes using semi-empirical self-consistent tight binding and ab-inito density functional methods. *Journal of Physics Communications, 4*(1), 015004.
29. Phuruangrat, A., Karthik, K., Kuntalue, B., Dumrongrojthanath, P., Thongtem, S., & Thongtem, T. (2019). Refuxing synthesis and characterization of ZnS nanoparticles and their photocatalytic properties. *Chalcogenide Letters, 16*, 387–393.
30. Kannnan, K., Radhika, D., Gnanasangeetha, D., Krishna, L. S., & Gurushankar, K. (2021). Y3+ and Sm3+ co-doped mixed metal oxide nanocomposite: Structural, electrochemical, photocatalytic, and antibacterial properties. *Applied Surface Science Advances, 4*, 100085.
31. Kannan, K., Radhika, D., Kasai, R., Gnanasangeetha, D., Palani, G., Gurushankar, K., Koutavarapu, R., Lee, D. Y., & Shim, J. (2022). Facile fabrication of novel ceria-based nanocomposite (CYO-CSO) via co-precipitation: Electrochemical, photocatalytic and antibacterial performances. *Journal of Molecular Structure, 1256*, 132519.
32. Kannnan, K., Radhika, D., Gnanasangeetha, D., Lakkaboyana, S., Sadasivuni, K., Gurushankar, K., & Hanafiah, M. (2021). Photocatalytic and antimicrobial properties of microwave synthesized mixed metal oxide nanocomposite. *Inorganic Chemistry Communications, 125*, 108429.
33. Singh, A., Kaushik, V., Chahal, S., Goswami, A., & Nain, S. (2021). Efficient Degradation of Methylene Blue Dye and Antibacterial Performance of Shape Controlled RuO2 Nanocomposites. *ChemistrySelect, 6*(37), 10038–10050.
34. Singh, A., Chahal, S., Dahiya, H., Goswami, A., & Nain, S. (2021). Synthesis of Ag nanoparticle supported graphene/multiwalled carbon nanotube based nanohybrids for photodegradation of toxic dyes. *Materials Express, 11*(6), 936–946.
35. Naito, M., Yokoyoma, T., Hosokawa, K., & Nogi, K. (2018). *Nanoparticle technology handbook* (3rd ed., pp. 109–168). Elsevier.
36. Liu, S., Ng, A. K., Xu, R., Wei, J., Tan, C., Yang, Y., & Chen, Y. (2010). Antibacterial action of dispersed single-walled carbon nanotubes on Escherichia coli and Bacillus subtilis investigated by atomic force microscopy. *Nanoscale, 2*, 2744–2750.
37. Banerjee, M., Mallick, S., Paul, A., Chattopadhyay, A., & Ghosh, S. S. (2010). Heightened reactive oxygen species generation in the antimicrobial activity of a three component iodinated chitosan−silver nanoparticle composite. *Langmuir, 26*(8), 5901–5908.
38. Santhoshkumar, A., Kavitha, H. P., & Suresh, R. (2016). Hydrothermal synthesis, characterization and antibacterial activity of NiO nanoparticles. *Journal of Advanced Chemical Sciences, 2*(2), 230–232.
39. Tamara, F. R., Lin, C., Mi, F., & Ho, Y. (2018). Antibacterial effects of chitosan/cationic peptide nanoparticles. *Nanomaterials, 8*, 1–15.
40. Kovach, K., Sabaraya, I., Patel, P., Kiristis, M., Saleh, N. B., & Gordon, V. (2020). Suspended multiwalled, acid-functionalized carbon nanotubes promote aggregation of the opportunistic pathogen Pseudomonas aeruginosa. *PLoS One, 15*(7), 1–5.
41. Maksimova, Y. G. (2019). Microorganisms and carbon nanotubes: interaction and applications. *Applied Biochemistry and Microbiology, 55*, 1–12.